Journal of Materials Chemistry A

RSC Publishing

PAPER

View Article Online
View Journal | View Issue

Cite this: J. Mater. Chem. A, 2013, 1, 11809

Influence of the N-heterocycle substituent of the dithieno[3,2-*b*:2′,3′-*d*]pyrrole (DTP) spacer as well as sensitizer adsorption time on the photovoltaic properties of arylamine organic dyes†

Zhihui Wang,[ab] Mao Liang,*[a] Yujie Hao,[a] Yue Zhang,[ab] Lina Wang,[a] Zhe Sun[a] and Song Xue*[a]

Received 16th July 2013
Accepted 30th July 2013

DOI: 10.1039/c3ta12746j

www.rsc.org/MaterialsA

Dithieno[3,2-*b*:2′,3′-*d*]pyrrole (DTP) compounds with strong electron-donating ability are promising spacers for photosensitizers. A series of new arylamine organic dyes bearing N-heterocycle-substituted DTP spacers has been designed and synthesized for iodine-free dye-sensitized solar cells (DSCs). The absorption, electrochemical, and photovoltaic properties for all the sensitizers have been systematically investigated. It was found that the incorporation of a dihexylaniline or hexylcarbazole unit, instead of a benzene unit, can notably retard the charge recombination at the titania–electrolyte interface, thus improving the cell photocurrent and photovoltage. Furthermore, we found a significant efficiency enhancement upon prolonging the adsorption time during the dye uptake from solution. When the dye adsorption was performed for 36 hours, the photovoltaic performance parameters measured under standard reporting conditions improved, in comparison to cells stained for 12 hours. The effects of adsorption time, correlated dye load amounts and electron lifetime were also scrutinized in terms of light-harvesting, interfacial kinetic parameters, as well as their joint contribution to the photovoltaic performance. Profiting from the favorable influence that the 36 hours dye uptake exerts on photovoltaic performance, we have realized a highly efficient iodine-free DSC displaying a power conversion efficiency of 8.20% measured at 100 mW cm^{-2} simulated AM1.5 conditions.

Introduction

Dye-sensitized solar cells (DSCs), as a new type of photovoltaic technology, have been considered to be a credible alternative to conventional inorganic silicon-based solar cells because of their ease of fabrication, high efficiency and cost-effectiveness since the report by O'Regan and Grätzel.[1] To achieve high solar power conversion efficiency, great research efforts are focused on designing and synthesizing new photosensitizers (*e.g.* Ru-based complexes,[2–5] zinc porphyrin complexes[6–8] and organic sensitizers[9–22]) as well as into the deep understanding of essential interface processes in DSCs.[23–25] Amongst these emerging photosensitizers, arylamine organic dyes with robust availability, ease of structural tuning and generally high molar extinction coefficients, have recently received great attention. So far, arylamine organic dyes have gained promising solar energy-to-electricity conversion efficiencies (PCE) that are comparable to Ru-based complexes.[9]

Aside from the electron donor (D) and acceptor (A) in a typical D–π–A system, the conjugated bridging segment (π) is widely recognized for its significance for the performance control of DSCs. Actually, the development of fused-ring building blocks as π-linkers for arylamine organic dyes has been proven to be a good strategy to enhance the efficiency of arylamine dyes. Representative fused-ring thiophenes reported to date include thienothiophenes,[26] benzodithiophenes (benzo[1,2-*b*:4,5-*b*′]dithiophene, BDT1;[27,28] benzo[2,1-*b*:3,4-*b*′] dithiophene, BDT2 (ref. 28 and 29)), and β,β′-bridged bithiophenes (dithienothiophenes, DTT;[30] dithieno[3,2-*b*:2′,3′-*d*]silole, DTS;[31] cyclopentadithiophene, CPDT[32,33]). It is noteworthy that organic dyes using the β,β′-bridged bithiophenes as a π-linker generally show a superior performance relative to those of benzodithiophenes. One of the major advantages of β,β′-bridged bithiophenes is their high electron-donating ability, strongly enhancing the photocurrent of devices. Therefore, the design and development of new fused-ring building blocks with high electron-donating ability is necessary and desired for the future development of DSCs. In a review on conjugated polymers for organic solar cells, You and co-workers

[a]Tianjin Key Laboratory of Organic Solar Cells and Photochemical Conversion, Department of Applied Chemistry, Tianjin University of Technology, Tianjin 300384, P.R. China. E-mail: liangmao717@126.com; xuesong@ustc.edu.cn

[b]Department of Chemistry, Tianjin University, Tianjin, 300072, P.R. China

† Electronic supplementary information (ESI) available: Syntheses and characterizations of new compounds, and optimized geometrical configuration of the dyes. See DOI: 10.1039/c3ta12746j

proposed an empirical chart showing the relative electron-donating ability of various donor units.[34] Dithieno[3,2-*b*:2′,3′-*d*]pyrrole (DTP) compounds are thought to have a stronger electron-donating ability than that of other fused-ring thiophene building blocks. Besides this, DTP also shows two favorable characteristics in the areas of dye preparation and performance: (i) not involving cryogenic temperatures and hazardous organolithium reagents; (ii) being able to easily tune the HOMO and LUMO energy levels, as well as the steric hindrance for organic dyes by the introduction of different substituents on the bridging nitrogen of DTP, which may lead to the synthesis of interesting DTP dyes with tailor-made photophysical, electrochemical, and other properties to fulfil these requirements for high performance DSCs. DTP derivatives therefore look to be important frameworks in functional organic dyes for DSCs. To date, several groups, including our group, have adopted DTP derivatives for constructing efficient organic dyes.[35–40] The results highlight the great potential of DTP for the development of tailored efficient arylamine organic dyes.

As part of our systematic investigation of fused-ring thiophene building blocks for organic dyes,[27,39,41] we report here three novel dihexylaniline, hexylcarbazole and hexylindoline substituted DTP chromophores, respectively named XS58, XS59 and XS60 (Fig. 1) for iodine-free DSCs. To reveal the influence of the N-heterocycle substituent of the DTP spacer on the performance of the dye-sensitized solar cells, the optical, electrochemical, and photovoltaic properties of these organic dyes were investigated. For comparison, XS61 featuring the phenyl substituted DTP linker was prepared as a reference.

In addition, we have also checked the effect of dye adsorption time on the performance of DSCs. To the best of our knowledge, the influence of adsorption time upon the efficiency of iodine-free DSCs, and the correlation between the adsorption time effect and dye structure, have received only limited attention to date. In this study, we found the beneficial effect of prolonging the adsorption time during the dye uptake from solution. The dyes (*i.e.* XS58 and XS59), with a strong ability to retard charge recombination, exhibit a significant efficiency enhancement when the dye adsorption was performed for 36 hours. This finding provides an important new insight into the effect of the dye structure on the photovoltaic performance of the iodine-free DSCs.

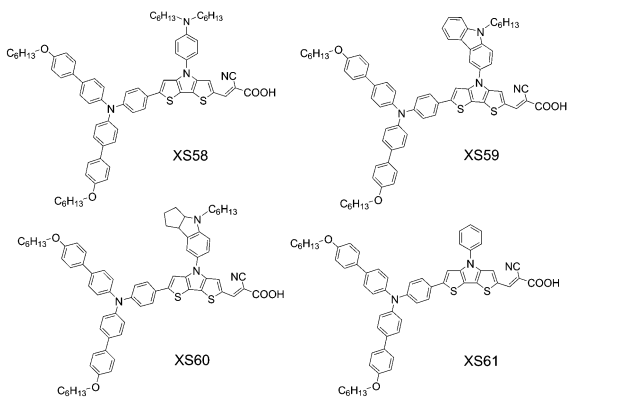

Fig. 1 Chemical structures of XS58–XS61.

Experimental

Materials and instruments

The synthetic routes for dyes XS58–61 are shown in Scheme 1. 3,3′-Dibromo-2,2′-bithiophene, *n*-butyllithium, $Pd(PPh_3)_4$, $Pd_2(dba)_3$, $SnBu_3Cl$, *t*-ButONa, BINAP and cyanoacetic acid were purchased from Energy Chemical (China). 4-Tertpyridine (TBP) and 0.1 M lithium bis(trifluoromethanesulfonyl)imide (LiTFSI) were purchased from Aldrich. *N*,*N*-Dimethylformamide was dried over and distilled from CaH_2 under an atmosphere of nitrogen. Phosphorus oxychloride was freshly distilled before use. Dichloromethane was distilled from calcium hydride under nitrogen atmosphere. All other solvents and chemicals used in this work were analytical grade and used without further purification.

^1H NMR and ^{13}C NMR spectra were recorded on a Bruker AM-300 or AM-400 spectrometer. The reported chemical shifts were against TMS. High resolution mass spectra were obtained with a Micromass GCT-TOF mass spectrometer. The melting point was taken on a RY-1 thermometer and the temperatures were uncorrected.

Optical and electrochemical measurements

The absorption spectra of the dyes and sensitized films were measured by a SHIMADZU UV-2600 spectrophotometer. Fluorescence measurements were carried out with a HITACHI F-4500 fluorescence spectrophotometer.

Cyclic voltammetry (CV) measurements for the sensitized films were performed on a Zennium electrochemical workstation (ZAHNER, Germany), with sensitized electrodes as the working electrode, Pt-wires as the counter electrode, and an

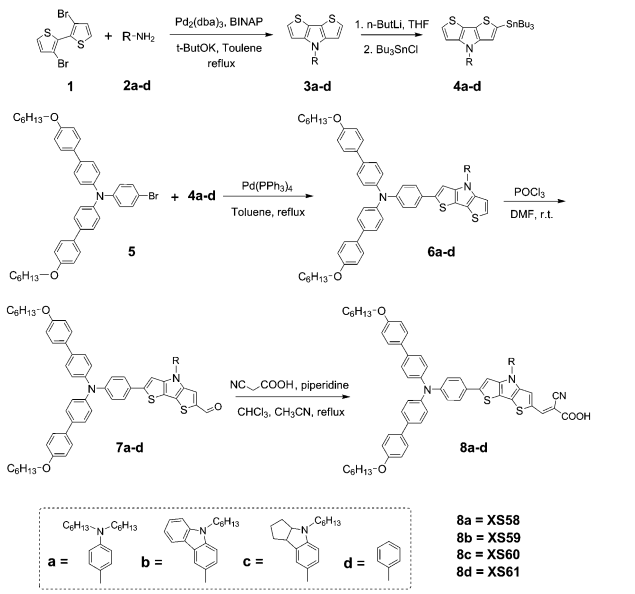

Scheme 1 Schematic diagram for the synthesis of the studied dyes.

Ag/AgCl electrode as the reference electrode at a scan rate of 50 mV s^{-1}. Tetrabutylammonium perchlorate (TBAP, 0.1 M) and MeCN were used as the supporting electrolyte and solvent, respectively. The results were calibrated using ferrocene as the standard.

Charge densities at open circuit and intensity modulated photovoltage spectroscopy (IMVS) were performed on a Zennium electrochemical workstation (ZAHNER, Germany), which includes a green light emitting diode (LED, 532 nm) and the corresponding control system. The intensity-modulated spectra were measured at room temperature with the light intensity ranging from 5 to 75 W m^{-2}, in a modulation frequency ranging from 0.1 Hz to 10 kHz, and with the modulation amplitude less than 5% of the light intensity.

Fabrication and characterization of DSCs

The TiO_2 paste (particle size, 20 nm) was printed on a conducting glass (Nippon Sheet Glass, Hyogo, Japan, fluorine-doped SnO_2 over layer, sheet resistance of 10 Ω sq^{-1}) using a screen printing technique. The film was dried in air at 120 °C for 30 min and calcined at 500 °C for 30 min under flowing oxygen before cooling to room temperature. The heated electrodes were impregnated with a 0.05 M titanium tetrachloride solution in a water-saturated desiccator at 70 °C for 30 min and fired again to give a *ca.* 3 μm thick mesoscopic TiO_2 film. The TiO_2 electrode was stained by immersing it into a 0.3 mM XS58–XS61 dye solution in a mixture of DCM–EtOH (v/v, 1 : 4) and kept at room temperature for 12, 36 and 48 hours. The sensitized electrodes were then rinsed with dry ethanol and dried by a dry air flow. Pt catalyst was deposited on the FTO glass by coating with a drop of H_2PtCl_6 solution (40 mM in ethanol) with the heat treatment at 395 °C for 15 min to give the photoanode. The sensitized electrode and Pt-counter electrode were assembled into a sandwich type cell by a 25 μm thick Surlyn (DuPont) hot-melt gasket and sealed up by heating. The cobalt electrolyte, E1, was composed of 0.25 M $[Co(II)(phen)_3](PF_6)_2$, 0.05 M $[Co(III)(phen)_3](PF_6)_3$, 0.5 M 4-tert-pyridine (TBP) and 0.1 M LiTFSI in acetonitrile. For comparison, an iodine electrolyte consisting of 0.25 M 1,2-dimethyl-3-*n*-propylimidazolium iodide (DMPImI), 0.1 M LiTFSI, 0.05 M I_2, and 0.5 M TBP in acetonitrile, namely E2, was formulated.

The photocurrent–voltage (J–V) characteristics of the solar cells were carried out using a Keithley 2400 digital source meter controlled by a computer and a standard AM1.5 solar simulator-Oriel 91160-1000 (300 W) Solar Simulator 2 × 2 Beam. The light intensity was calibrated by an Oriel reference solar cell. A metal mask with an aperture area of 0.2 cm^2 was covered on a testing cell during all measurements. The action spectra of monochromatic incident photon-to-current conversion efficiency (IPCE) for the solar cells were performed by using a commercial setup (QTest Station 2000 IPCE Measurement System, CROWNTECH, USA).

Synthesis

The synthesis of the intermediates of XS58–XS61 can be found in the ESI.† The synthesis of the XS58–XS61 dyes are described as follows.

General synthesis procedure of the dyes. To a stirred solution of compound **7a** (0.1 mmol) and cyanoacetic acid (0.15 mmol) in acetonitrile (6 mL) was added chloroform (3 mL) and piperidine (0.3 mmol). The reaction mixture was refluxed for 8 hours. Additional cyanoacetic acid (0.1 mmol) and piperidine (0.2 mmol) were added. The mixture was refluxed continuously for 8 hours and then acidified with 1 M hydrochloric acid aqueous solution (15 mL). The crude product was extracted into CH_2Cl_2, washed with water, and dried over anhydrous $MgSO_4$. After removing the solvent under reduced pressure, the residue was purified by column chromatography to give the target dyes.

Synthesis of 8a (XS58). Red power (58% yield). Mp: 152–155 °C. IR (KBr): 3426, 2956, 2925, 1736, 1609, 1463, 1377, 1283, 1019, 821 cm^{-1}. ^{1}H NMR (400 MHz, DMSO-d_6): δ 8.49 (s, 1H), 8.05 (s, 1H), 7.74–7.63 (m, 3H), 7.53–7.48 (m, 9H), 7.39 (d, J = 8.2 Hz, 2H), 7.06 (d, J = 8.2 Hz, 4H), 6.99 (d, J = 8.2 Hz, 2H), 6.91 (d, J = 8.2 Hz, 4H), 6.75 (d, J = 8.4 Hz, 2H), 3.91 (t, J = 8.2 Hz, 4H), 3.29 (m, 4H), 1.70–1.62 (m, 4H), 1.53–1.38 (m, 8H), 1.29–1.23 (m, 20H), 0.91–0.86 (m, 12H). ^{13}C NMR (100 MHz, pyridine-d_5): 160.2, 151.3, 150.2, 149.1, 148.9, 147.2, 145.6, 137.3, 136.9, 136.5, 136.3, 135.9, 135.1, 133.9, 130.2, 129.1, 128.9, 128.1, 127.8, 126.4, 126.3, 126.0, 124.9, 123.9, 116.4, 115.8, 113.7, 108.8, 69.2, 55.9, 32.9, 32.7, 30.4, 28.5, 27.9, 26.9, 23.9, 23.7, 15.1, 15.0. HRMS (ESI) calcd for $C_{72}H_{80}N_4O_4S_2$ (M + H^+): 1129.5699, found: 1129.5662.

Synthesis of 8b (XS59). Red power (75% yield). Mp: 160–163 °C. IR (KBr): 2956, 2924, 2850, 1675, 1603, 1462, 1377, 1022, 820 cm^{-1}. ^{1}H NMR (400 MHz, DMSO-d_6): δ 8.51 (s, 1H), 8.46 (d, J = 1.4 Hz, 1H), 8.27 (d, J = 7.6 Hz, 1H), 8.16 (s, 1H), 7.80 (d, J = 8.8 Hz, 1H), 7.73–7.65 (m, 4H), 7.60 (s, 1H), 7.53–7.50 (m, 9H), 7.22 (t, J = 7.4 Hz, 1H), 7.07 (d, J = 8.4 Hz, 4H), 7.0 (d, J = 8.4 Hz, 2H), 6.93 (d, J = 8.4 Hz, 4H), 4.45 (t, J = 6.4 Hz, 2H), 3.94 (t, J = 6.4 Hz, 4H), 1.83–1.76 (m, 2H), 1.73–1.66 (m, 4H), 1.42–1.38 (m, 4H), 1.31–1.23 (m, 14H), 0.88 (t, J = 6.8 Hz, 6H), 0.81 (t, J = 6.4 Hz, 3H). ^{13}C NMR (100 MHz, pyridine-d_5): 159.0, 150.2, 149.1, 147.9, 146.1, 144.7, 141.5, 139.5, 136.1, 135.8, 135.4, 135.1, 134.7, 134.1, 132.8, 130.5, 129.0, 127.9, 127.7, 127.0, 126.9, 125.3, 123.8, 123.7, 123.4, 123.1, 122.7, 122.1, 121.2, 119.6, 116.2, 115.2, 115.0, 110.3, 109.7, 107.7, 68.0, 43.1, 31.5, 29.3, 29.1, 26.8, 25.8, 22.6, 22.5, 13.9, 13.8. HRMS (ESI) calcd for $C_{72}H_{70}N_4O_4S_2$ (M + H^+): 1119.4917, found: 1119.4961.

Synthesis of 8c (XS60). Red power (91% yield). Mp: 194–198 °C. IR (KBr): 3423, 2928, 2856, 1676, 1571, 1495, 1246, 1137 cm^{-1}. ^{1}H NMR (400 MHz, DMSO-d_6): δ 8.52 (s, 1H), 8.06 (s, 1H), 7.67 (d, J = 8.4 Hz, 2H), 7.55–7.49 (m, 9H), 7.19–7.17 (m, 2H), 7.09 (d, J = 8.4 Hz, 4H),7.01 (d, J = 8.4 Hz, 2H), 6.93 (d, J = 8.4 Hz, 4H), 6.40 (d, J = 8.8 Hz, 1H), 4.27–4.24 (m, 1H), 3.94 (t, J = 6.4 Hz, 4H), 3.77–3.73 (m, 1H), 3.5–3.48 (m, 1H), 3.26–3.19 (m, 2H), 3.13–3.06 (m, 1H), 2.02–1.95 (m, 1H), 1.85–1.75 (m, 2H), 1.73–1.62 (m, 5H), 1.57–1.49 (m, 2H), 1.44–1.37 (m, 4H), 1.32–1.30 (m, 14H), 0.90–0.87 (m, 9H). ^{13}C NMR (100 MHz, pyridine-d_5): 159.0, 151.8, 150.2, 149.1, 147.9, 146.1, 144.7, 136.1, 135.8, 135.6, 135.4, 135.1, 134.7, 133.9, 132.8, 129.1, 127.9, 127.7, 127.6, 126.9, 125.3, 123.7, 123.4, 123.1, 122.7, 120.4, 115.3, 114.5, 107.8, 105.0, 69.4, 68.0, 46.4, 45.7, 35.5, 33.4, 31.7, 31.5, 29.3, 27.3, 26.9, 25.8, 24.6, 22.7, 22.6,

14.0, 13.9. HRMS (ESI) calcd for $C_{71}H_{74}N_4O_4S_2$ (M + H^+): 1111.5229, found: 1111.5166.

Synthesis of 8d (XS61). Red power (89% yield). Mp: 152–154 °C. IR (KBr): 3441, 2924, 2856, 1678, 1570, 1495, 1400, 1249, 821. ^{1}H NMR (400 MHz, DMSO-d_6): 8.46 (s, 1H), 8.17 (s, 1H), 7.75–7.71 (m, 4H), 7.68–7.62 (m, 3H), 7.58–7.53 (m, 8H), 7.48–7.44 (m, 1H), 7.11 (d, J = 8.4 Hz, 4H), 7.05 (d, J = 8.4 Hz, 2H), 6.95 (d, J = 8.4 Hz, 4H), 3.95 (t, J = 6.4 Hz, 4H), 1.74–1.67 (m, 4H), 1.43–1.38 (m, 4H), 1.32–1.30 (m, 8H), 0.88 (t, J = 6.4 Hz, 6H). ^{13}C NMR (100 MHz, pyridine-d_5): 159.1, 150.2, 149.1, 148.5, 148.0, 146.9, 146.1, 143.4, 138.8, 136.2, 135.8, 135.4, 135.1, 134.7, 134.4, 132.8, 130.2, 128.9, 127.7, 127.0, 125.3, 123.7, 122.7, 115.8, 115.3, 107.7, 73.5, 31.5, 29.3, 25.8, 22.6, 13.9. HRMS (ESI) calcd for $C_{60}H_{55}N_3O_4S_2$ (M + H^+): 946.3712, found: 946.3798.

Results and discussion

The synthetic routes to XS58–61 are shown in Scheme 1. Our synthesis started from the Buchwald–Hartwig amination of 3,3′,5,5′-tetrabromo-2,2′-bithiophene **1** and arylamines **2a–d** to afford the key intermediates dithieno[3,2-*b*:2′,3′-*d*]pyrrole **3a–d**. Treatment of the crucial intermediate **3a–d** with *n*-BuLi, followed by quenching with Bu_3SnCl and then reaction with compound **5** gave the products **6a–d**. Aldehydes **7a–d** were synthesized in excellent yield by Vilsmeier–Haack reaction of **6a–d** with $POCl_3$ and DMF. Subsequently, the target dyes were obtained in good yields *via* Knoevenagel condensation reaction of the respective aldehydes with cyanoacetic acid in the presence of a catalytic amount of piperidine.

UV-vis absorption properties

The UV-vis absorption spectra of the dyes in CH_2Cl_2 solutions are depicted in Fig. 2a. The optical and electrochemical properties of the dyes are summarized in Table 1. The absorption spectra of XS58–XS61 exhibit an intense peak around 525 nm, which can be assigned to the intramolecular charge transfer transitions from the triarylamine donor to the cyanoacrylic acid acceptor. It is worth noting that XS58–XS61 have high molar extinction coefficients (54 900 to 64 200 M^{-1} cm^{-1}) and ensure excellent light harvesting. DSCs based on cobalt redox couples are therefore convenient, where the use of thinner than usual TiO_2 film thicknesses is preferred to overcome mass transport and recombination limitations associated with the polypyridyl cobalt redox shuttles.[42,43] The broad absorption response, as well as the high molar extinction coefficients observed for XS58–XS61, can be attributed to the planar configuration of the fused-ring DTP units.

Table 1 Photophysical data for the studied dyes

Dye	λ_{max}[a]/nm (ε/10^3 M^{-1} cm^{-1})	E_{0-0}[b]/V	$E_{D/D+}$[c]/V	$E_{D^*/D+}$[d]/V
XS58	341 (39), 524 (54.9)	2.17	1.07	−1.10
XS59	345 (44.4), 521 (60.9)	2.15	0.99	−1.16
XS60	343 (41.4), 527 (60.5)	2.16	1.01	−1.15
XS61	346 (44.2), 522 (64.2)	2.14	0.98	−1.16

[a] The absorption spectra in DCM. [b] E_{0-0} values were estimated from the intersections of normalized absorption and emission spectra (λ_{int}): E_{0-0} = 1240/λ_{int}. [c] $E_{D/D+}$ was recorded by cyclic voltammograms of the dye-loaded TiO_2 film. [d] $E_{D^*/D+}$ was calculated from $E_{D/D+}$ − E_{0-0}.

Electrochemical properties

The electrochemical properties of the four dyes were investigated by using cyclic voltammetry (Fig. 3). The oxidation potentials ($E_{D/D+}$, taken as the HOMO levels of the dyes) of XS58, XS59, XS60 and XS61 were measured to be 1.07, 0.99, 1.01, and 0.98 V *versus* normal hydrogen electrode (NHE), respectively. Note that, the XS59 dye has a negatively shifted HUMO in comparison with XS58 and XS60, suggesting the feature of being electron-richer for hexylcarbazole substituted DTP, in contrast to the dihexylaniline, and hexylindoline substituted DTP. Unexpectedly, the HOMO level of XS61 is slightly lower than that of XS59. Nevertheless, the low HOMO level does not always induce a high photocurrent, which is limited by many factors, such as the dye load amount, electron injection efficiency, and electron collection. For example, although the HOMO level for XS61 is slightly lower than those for XS58 and XS59, XS61 the sensitized cell exhibits a distinct attenuated incident photon-to-electron conversion efficiency (IPCE) action spectrum compared to its XS58 and XS59 counterparts (see the next section).

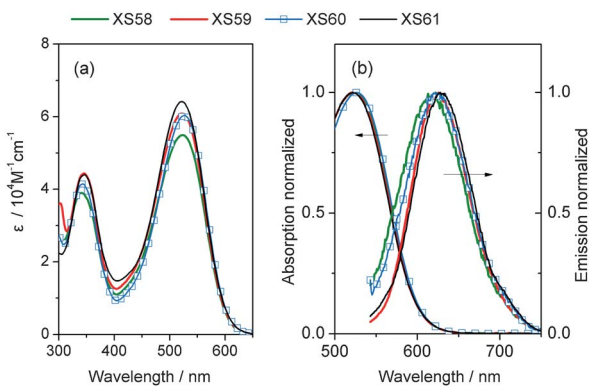

Fig. 2 Absorption spectra of XS58–XS61 in DCM.

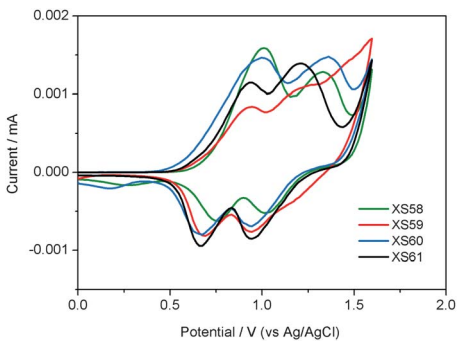

Fig. 3 Cyclic voltammograms of the dye-coated titania films.

As shown in Fig. 4, the HOMO levels of XS58–XS61 are more positive than the $[Co(II/III)(phen)_3]^{n+}$ (phen = 1,10-phenanthroline) and I^-/I_3^- redox couples (0.62 V and 0.4 V *vs.* NHE, respectively). In the cobalt control cells, the calculated driving forces for the dye regeneration of XS58, XS59, XS60, and XS61 were 0.45, 0.37, 0.39, and 0.36 eV, respectively. Considering the fact that the cobalt control cells presented comparable J_{SC} values related to that of the iodine control cells (see next section), it can be said that the driving forces in the cobalt control cells were sufficient to regenerate most of these dyes.

The excited-state potential (E_{D^*/D^+}), reflecting the LUMO level of the dye, can be derived from the ground-state oxidation potential and the zero–zero excitation energy (E_{0-0}) determined from the intersection of the absorption and emission spectra. The LUMO of the four dyes were calculated to be −1.10, −1.16, −1.05, and −1.16 V, respectively, indicative of the thermodynamic feasibility for electron injection to the conduction band (E_{CB}) of TiO_2 (−0.5 V *versus* NHE).

Theoretical calculations

To gain further insight into the molecular structure and electron distribution of these dyes, TDDFT excited states calculations at the B3LYP/6-31G level *in vacuo* with the B3LYP/6-31G optimized ground-state geometries were performed. The transitions of XS58–XS61 with oscillator strengths (f) above 0.5 are summarized in Table 2. The electron distributions of the HOMO and LUMO of XS58–XS61 are similar. The HOMO is populated over the triphenylamine donor and DTP units with considerable contribution from the former, while the LUMO is delocalized through the fused thiophene units and cyanoacrylic acid fragments with sizable contribution from the latter. The HOMO–LUMO excitation moves the electron distribution from the donor unit to the cyanoacrylic acid moiety, thus allowing an efficient photoinduced electron transfer from the dye to the TiO_2 electrode under light irradiation. TDDFT calculations disclose that the low-energy absorption bands of XS58, XS59 and XS60 can be assigned to two or three charge-transfer excitations (see Table 2), in contrast to only one charge transfer excitation (HOMO to LUMO) in XS61. Besides the HOMO to LUMO excitation, the low-energy absorption bands of XS58–XS60 are correlated with the HOMO-2 to LUMO and HOMO-1 to LUMO excitations.

It is also worth noting that there is nearly no electron distribution of the HOMO on the DTP substituents in these dyes. This observation was also reported by Wang and co-workers. They proposed that 2′,6′-bis(octyloxy)-biphenyl and hexyl substituted DTP could be considered as an insulating spacer to reduce the intermolecular exciton annihilation in the assembly of dye molecules grafted on the surface of titania.[36–38] It seems that the lowest-energy absorption band of the DTP dyes could not be tuned by alternation of the substituents.

However, when carefully comparing the frontier molecular orbitals of XS59 and XS60 between HOMO and HOMO-1, a district electron distribution of HOMO-1 on the hexylcarbazole and hexylindoline was interestingly observed (Fig. 5). In particular, the electron distribution of HOMO-1 was mainly populated over hexylindoline substituted DTP in the case of XS60. This suggests that the introduction of N-heterocycle into the DTP unit could impact the charge-transfer excitation of the dyes, offering the opportunity to tune the physicochemical properties of the titania–dye–electrolyte interface and thereby modulate the photovoltaic parameters of dye-sensitized solar cells.

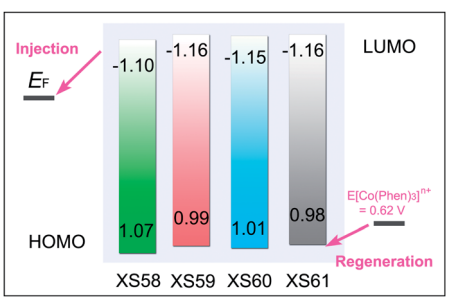

Fig. 4 Energy diagram of the dyes.

Photovoltaic performance of the DSCs

Recent studies have highlighted the importance of the exploration of bulky arylamine dyes with high extinction coefficients for iodine-free dye-sensitized solar cells.[32,33,42–45] Amongst all the iodine-free liquid electrolytes, so far only the cobalt redox couples have shown impressively high efficiencies comparable to iodide/triiodide electrolyte by using organic dyes.[46,47] Fig. 6a shows the incident-photon-to-current conversion efficiency (IPCE) of DSCs made from thin titania films stained with dyes for 36 hours, in combination with the tris(1,10-phenanthroline)cobalt(II)/(III) redox couple (E1). The four cells exhibit a broad plateau from 450 to 600 nm, implying a nice light absorption in this wavelength range. It is noted that at a given wavelength, the XS58, XS59 and XS61 cells exhibit an obviously higher IPCE value than XS60. To clarify the origin of the IPCE attenuation of XS60, we have measured the amounts adsorbed on the TiO_2 film. By comparing the absorbance change of a dye solution before and after the dye up-taking with a titania film, the surface coverages (Γ) of XS58, XS59, XS60 and XS61 were determined to be 0.64×10^{-7}, 0.80×10^{-7}, 0.45×10^{-7} and 0.76×10^{-7} mol cm^{-2}, respectively. The lower surface coverage of XS60 is partially responsible for its reduced IPCE. Nevertheless, it is necessary to point out that the adsorption amount of dyes is not the sole determinant. Other factors, such as the overall electron injection efficiency (Φ_{inj}), driving force ΔG^0 for regeneration of dyes and the charge collective efficiency (η_{col}) should be considered. For example, the IPCE maximum of the XS61 is far behind that of XS59, though the adsorption amount of the former is slightly lower than that of the latter. It can be found that the E_{D^*/D^+} and E_{D/D^+} of XS59 and XS61 are very similar, indicating comparable electron injection efficiency and driving force required for the regeneration of the photooxidized dye. Therefore, the dissimilarity of IPCE observed for XS59 and XS61 could be attributable to the variation of charge collective efficiency (see the next section).

Table 2 Calculated details of the electronic transitions of the dyes with relative oscillator strengths larger than 0.5

Dye	State	Calculated energy (eV, nm)	Oscillator strength (f)	Transition assignment[a]
XS58	1	2.13, 580	0.97	H → L (86%) H-2 → L (2.6%)
	3	2.81, 440	1.02	H-2 → L (77%) H → L + 1 (6.1%)
XS59	1	2.10, 589	0.96	H → L (87%) H-1 → L (2.2%)
XS60	2	2.13, 581	0.98	H → L (83%) H-1 → L (3.6%) H-2 → L (2.6%)
	3	2.80, 441	0.99	H-2 → L (77%) H → L + 1 (5.9%)
XS61	1	2.06, 600	0.91	H → L (88%)

[a] H means HOMO, and L means LUMO.

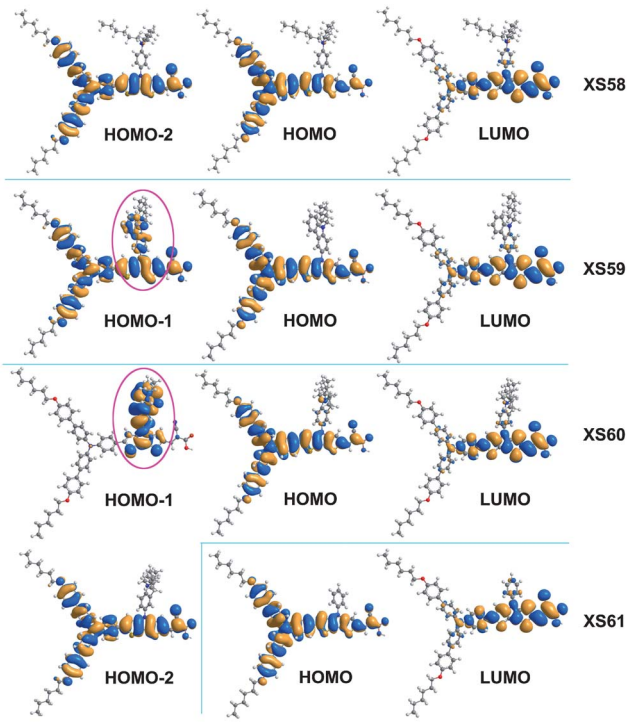

Fig. 5 Frontier molecular orbitals of the dyes. The isodensity surface values were fixed at 0.2.

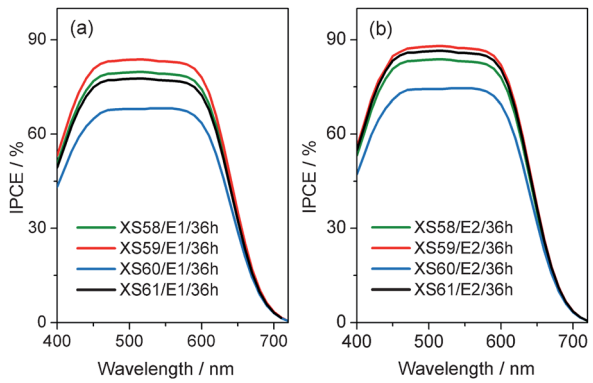

Fig. 6 IPCE action spectra of the studied DSCs employing cobalt electrolyte (a) and iodine electrolyte (b).

We further recorded the J–V curves of the cells made from XS58, XS59, XS60, and XS61 in combination with a tris(1,10-phenanthroline)cobalt(II/III) redox shuttle (E1) under AM1.5 irradiation (100 mW cm^{-2}), and the detailed parameters are collected in Table 3. The cobalt electrolyte was composed of 0.25 M $[Co(II)(phen)_3](PF_6)_2$, 0.05 M $[Co(III)(phen)_3](PF_6)_3$, 0.5 M 4-tertpyridine (TBP) and 0.1 M lithium bis-(trifluoromethanesulfonyl)imide (LiTFSI) in acetonitrile. As Fig. 7 presents, the short-circuit photocurrent density (J_{SC}), open-circuit photovoltage (V_{OC}), and fill factor (FF) of the XS61 cell were 12.1 mA cm^{-2}, 856 mV, and 0.67, respectively, affording a power conversion efficiency (PCE) of 6.94%. It was also found

Table 3 Photovoltaic parameters for the DSCs studied[a]

Dye	J_{SC}/mA cm^{-2}	V_{OC}/mV	FF	PCE (%)	Time (h)
XS58–E1	12.3	900	0.68	7.53	12
XS59–E1	12.8	870	0.69	7.68	12
XS60–E1	10.5	832	0.66	5.76	12
XS61–E1	12.0	849	0.67	6.83	12
XS58–E1	12.6	950	0.68	8.14	36
XS59–E1	13.3	907	0.68	8.20	36
XS60–E1	10.5	844	0.66	5.85	36
XS61–E1	12.1	856	0.67	6.94	36
XS58–E1	12.5	944	0.66	7.79	48
XS59–E1	13.1	903	0.67	7.92	48
XS60–E1	10.3	856	0.65	5.73	48
XS61–E1	11.9	862	0.65	6.56	48
XS58–E2	13.1	770	0.64	6.45	36
XS59–E2	13.8	764	0.66	6.96	36
XS60–E2	11.7	754	0.66	5.82	36
XS61–E2	13.5	721	0.65	6.33	36

[a] Measurements were performed under AM1.5 irradiation of the devices.

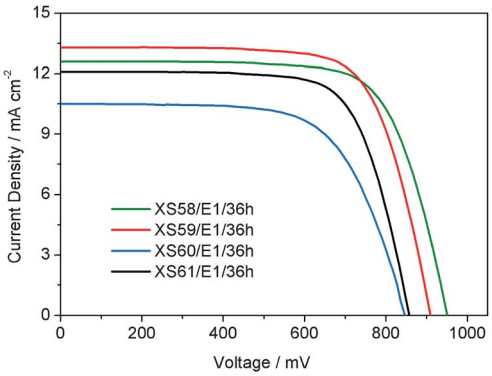

Fig. 7 *J–V* curves of the DSC devices studied employing the cobalt electrolyte under AM1.5G simulated solar light (100 mW cm^{-2}).

that the PCE of XS58 and XS59 is notably greater than that of its phenyl substituted DTP counterpart XS61, a result that is attributed to the greatly enhanced photocurrent or photovoltage. For instance, a notably improved J_{SC} of 13.3 mA cm^{-2} concomitant with an increased V_{OC} of 907 mV were achieved with the XS59 dye, contributing to a higher PCE of 8.20%. Under the same conditions, the DSC based on XS58 offered a J_{SC} of 12.6 mA cm^{-2}, a V_{OC} of 950 mV, and a FF of 0.68, corresponding to a PCE of 8.14%. In contrast, the XS60 cell presents lower PCE values than its XS58 and XS59 counterparts, primarily owing to the relatively low photocurrent, 10.5 mA cm^{-2}. Note that there was no scattering layer used in the fabrication of DSCs, which is one of the main reasons that the performance of the DSCs shown in this work is not higher than that reported in the literature. However, in view of the same conditions of the test, our approach is reliable for fair evaluation of the photovoltaic performance of the four dyes discussed in this work.

The *J–V* curves (Fig. 8) of these cells employing an iodine electrolyte consisting of 0.6 M DMPImI, 0.1 M LiTFSI, 0.03 M I_2 and 0.5 M TBP in acetonitrile for comparison (E2), were also measured under the irradiance of 100 mW cm^{-2}, simulated AM1.5 sunlight, and the detailed cell parameters are compiled in Table 3. The J_{SC}, V_{OC}, and FF of the XS59 sensitized DSC with the iodine electrolyte are 13.8 mA cm^{-2}, 764 mV, and 0.66,

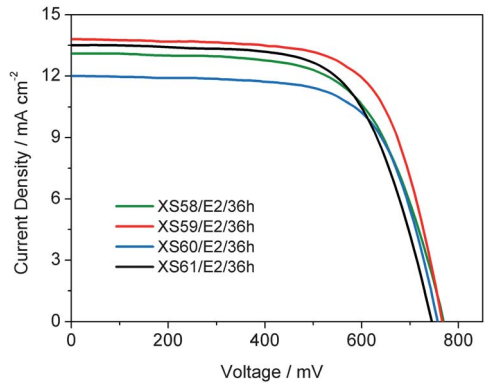

Fig. 8 *J–V* curves of studied DSC devices employing the iodine electrolyte under AM1.5G simulated solar light (100 mW cm^{-2}).

respectively, affording a PCE of 6.96%. In keeping with the IPCE measurements presented in Fig. 6b, the J_{SC} values of the iodine cells are slightly higher than those of the cobalt cells. In spite of this, the cobalt cells based on XS58 and XS59 display a significantly improved efficiency, in comparison to those of the iodine cells. The efficiency gain is primarily due to a significant increase in the V_{OC}, which compensates for a slight drop in the J_{SC}. The results indicate that the XS58 and XS59 dyes featuring high molar extinction coefficients and bulky DTP bridges are suitable for the DSCs employing the cobalt electrolyte. The validity of this analysis could be further examined by carefully comparing the electrolyte correlated J_{SC} variation for these dyes. It can be found that the 1.4 mA cm^{-2} increase of J_{SC} caused by the electrolyte alteration from cobalt to iodine for XS61 is much higher than those of XS58 and XS59 (0.5 mA cm^{-2}). As a result, XS61 displayed a slightly lower efficiency (1.89–5.7%) in comparison to that of XS58 and XS59 in the iodine electrolyte system, sharply contrasting with the distinct efficiency decrease (17.3–18.1%) in the cobalt electrolyte system. We therefore propose that organic dyes with bulky bridges should be preferred in the future development of organic dyes for DSCs employing the cobalt electrolyte.

Dependence of the photovoltage on the conduction band movement and charge recombination

To dissect the origins of the V_{OC} difference, possible factors influencing the V_{OC} for DSCs based on the four dyes involving the conduction band (CB) movement and the free electron density (n_c) in TiO_2 will be discussed in detail in the following sections.

In this work, charge densities at open-circuit, measured by the charge extraction technique,[48] were used to compare the conduction band positions in different DSCs. The electron lifetimes at open circuit (τ), measured by controlled intensity modulated photovoltage spectroscopy (IMVS), can be obtained by fitting either the real or imaginary part of the IMVS response (eqn (1) and (2)).[49,50]

$$\mathrm{re}(\Delta V_{OC}) = \frac{X_1}{1 + (\omega\tau^{re})^2} \quad (1)$$

$$\mathrm{im}(\Delta V_{OC}) = -\frac{X_2\omega\tau^{im}}{1 + (\omega\tau^{im})^2} \quad (2)$$

where $\mathrm{im}(\Delta V_{OC})$ is the imaginary modulation of the photopotential (ΔV_{OC}), $\mathrm{re}(\Delta V_{OC})$ is the real modulation of the photopotential (ΔV_{OC}), X_1, X_2, τ^{re} and τ^{im} are the fit parameters, and ω is the circular frequency of the light modulation.

Fig. 9a shows the relation between the V_{OC} and extracted charge density (Q) at open circuit. It can be found that for DSCs based on XS58, XS59, XS60 and XS61, the V_{OC} increases linearly with the logarithm of Q and all the curves have almost identical slopes. The three types of cell made with XS58, XS59, and XS60 display a similar extracted electron density at the same potential bias, indicative of a fixed conduction-band edge of titania with respect to the electrolyte Fermi-level. As compared to XS58, XS59, and XS60, XS61 showed a downward CB shift by 8 mV.

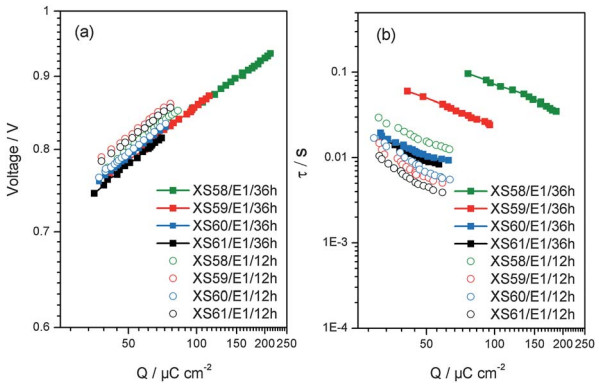

Fig. 9 Open circuit voltage (a) and electron lifetime (b) as a function of charge density for the DSCs studied.

The positive shift of CB was likely to be caused by a high dye load amount of XS61.

Evidently, the small CB shift observed could not explain the large V_{OC} improvement (63–98 mV) for the DSCs based on XS58 and XS59 in comparison to those of XS60 or XS61. Fig. 9b shows the electron lifetime as a function of Q for the DSCs based on XS58–XS61. At a fixed charge density, the electron lifetimes for the DSCs based on XS58 and XS59 are larger than that for the XS60 or XS61 based DSC by around 8- and 4-fold, respectively, which are in good agreement with their V_{OC} performances. As a result, the significant enhancement of the V_{OC} values observed for XS58 and XS59 was largely because of the increased electron lifetimes (*i.e.*, retarded electron recombination rate) rather than the different positions of the conduction band edge of TiO_2. It is noted that, the controlled charge recombination contributes to, not only the V_{OC}, but also the J_{SC} because of the improved charge collection efficiency at the photoanode, giving an explanation of the different IPCE values yielded by the DSCs based on XS59 and XS61.

Dependence of the photovoltaic performance of the devices on the time of film soaking

It is known that the dye load amount, as well as the packing of the dye molecules on TiO_2 film, has a significant influence on some key photovoltaic features, such as the photocurrent and photovoltage. Preliminary reports have highlighted the importance of the dye-bath solvents employed and the adsorption temperatures on the dye load amount, as well as the packing of the dyes.[51,52] Besides the two factors aforementioned, the effect of the soaking time on the performance of DSCs is also an area of concern. So far, there have been surprisingly few investigations, where the dye adsorption time was varied above 24 hours to check its effect on the solar cell output, especially regarding the cobalt cells. 12, 36 and 48 hours were subsequently employed to examine the behavior of a DSC whose sensitizer was adsorbed over 24 hours. Table 3 shows the device characteristics, *i.e.*, V_{OC}, J_{SC}, FF, and PCE under standard AM1.5 sunlight and for different times of dyes adsorption. Note that the values reported in this table represent an average of the measurements conducted on different cells.

As presented in Fig. 10, we recorded the J_{SC}, V_{OC}, FF, and PCE variation of cells for three different adsorption times. A significant effect of the dye adsorption time on the dye sensitized solar cell using XS58 and XS59 sensitized nanocrystalline titania films was seen. Close comparison of the photovoltaic parameters recorded reveals that the effect becomes particularly pronounced for dye sensitized films with 36 hours adsorption. Take XS59 for instance, the V_{OC} values obtained were 870 and 907 mV for adsorption times of 12 and 36 hours, respectively. This increase was accompanied by a significant improvement in the values of the J_{SC} from 12.8 to 13.3 mA cm^{-2}, and the PCE from 7.68 to 8.20%. A similar evolution was observed for the cells sensitized with XS58. A notably improved V_{OC} of 950 mV, concomitant with an increased J_{SC} of 12.6 mA cm^{-2} was achieved, contributing to a high PCE of 8.14%. This important observation indicates that tuning the adsorption time can notably impact the efficiency of the cells employing the cobalt electrolyte.

In sharp contrast to XS58 and XS59, the performance of XS60 and XS61 were furthermore found to be only weakly dependent upon the dye adsorption time. To clarify the different performances of the dyes, we focused on the adsorption times with the most contrasting photovoltaic performances, *i.e.* 12 and 36 hours. The relative conduction band positions and electron lifetimes of the corresponding DSCs were investigated (Fig. 9). The absorption spectra of the sensitized electrodes based on XS58–XS61 were also recorded (Fig. 11) to show the dye load amount variation (Table 4) for different adsorption times.

As shown in Table 4, the 36 hour cells showed a downward CB shift (5–32 mV) in contrast to their 12 hours counterparts. Rühle *et al.* proposed that the changes in surface potential (ΔE_c) can be estimated by[53]

$$\Delta E_c = \frac{N\mu \cos\theta}{\varepsilon\varepsilon_0} \quad (3)$$

where N is the coverage of dipoles, $\mu \cos\theta$ is the dipole (μ) component normal to the surface, ε_0 is the permittivity of the dipole layer, and ε is the vacuum permittivity. Considering that the $\mu \cos\theta$ would not change strongly in the DSCs with a fixed dye, the ΔE_c is therefore governed by the coverage of dipoles.

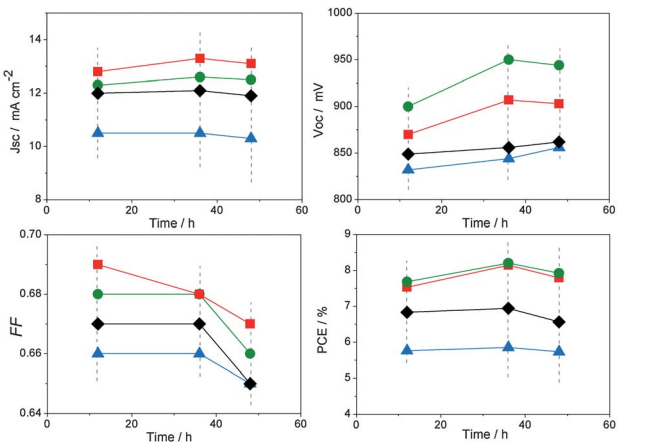

Fig. 10 J_{SC}, V_{OC}, FF, and PCE values of the DSCs based on XS58 (green), XS59 (red), XS60 (blue) and XS61 (black) as a function of adsorption time.

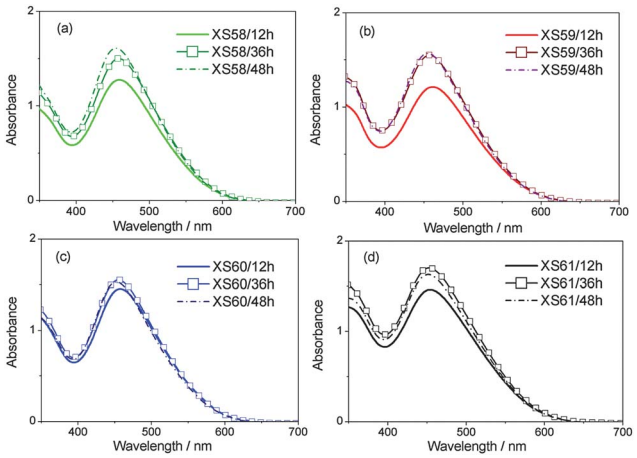

Fig. 11 Absorption spectra of the sensitized electrodes stained for 12, 36, and 48 hours.

As shown in Fig. 11, the 36 hours cells exhibit higher absorption peaks than those for the 12 hour cells, a result that is attributed to the enhanced dye coverage. Apparently, the E_{CB} of the 36 hour cells should become more negative than the latter. However, this deduction is not in accordance with the E_{CB} measurement, indicating other effects might be at work. According to the absorption measurements, there should be some titania uncovered by the dyes for the films stained for 12 hours. It is likely that the surface area of the naked TiO_2 could effectively interact with the electrolyte additive TBP, which has been reported to have a strong capacity to lift-up the titania conduction band edge. The dye load amount augmentation, along with the change of adsorption time from 12 hours to 36 hours, could reduce the amount of TBP that was adsorbed on the surface of titania, and the measured E_{CB} was thus shifted positively.

Based on the aforementioned analysis of the CB shifts, we thus concluded that the V_{OC} improvements of the 36 hour cells relative to the 12 hour cells were attributed to the retardation of charge recombination, rather than the position of the CB. To prove the validity of this assumption, we compared the electron lifetimes of the 36 hour cells with those of the 12 hour cells. At a fixed charge density (50 μC cm^{-2}), the electron lifetimes for the 36 hour cells based on XS58 and XS59 were larger than those for the 12 hours cells by around 10- and 8.7-fold, respectively. This indicates that the charge recombination between the electrons in the TiO_2 film and electron acceptors in the electrolyte was significantly retarded by dyes XS58 and XS59 with 36 hours adsorption, as compared to those with 12 hours adsorption. In contrast, the electron lifetimes for the 36 hour cells based on XS60 and XS61 were only 1.5- and 2.0-fold larger than that for the 12 hours cells, respectively. Not surprisingly, the photovoltage and photocurrent improved slightly due to the small change of the charge recombination rate.

It is worth noting that the weakened adsorption time effect for XS60 and XS61 did not arise from the variation of the dye load amount. As a matter of fact, we can distinguish diverse absorption features of the dye sensitized films for different absorption times. Taking XS61 for example, the dye load amount increased by 1.19-fold from 0.64×10^{-7} mol cm^{-2} for 12 hours adsorption to 0.76×10^{-7} mol cm^{-2} for 36 hours adsorption, which is higher than that of XS58 (1.14-fold). However, the electron lifetime improvement caused by prolonging the adsorption time for XS61 was much lower (5-fold) than that for XS58. Furthermore, although the 1.07-fold enhanced XS60 load amount was slightly less than that of XS58, this cannot be the only cause for the significantly weakened electron lifetime enhancement. We thus conclude that the dye load amount is not the key determinant of the degree of adsorption time effect. For a comparable dye load amount increasing, it is likely that the stronger ability of the retarding charge recombination of XS58/XS59 relative to XS60/XS61 plays a pivotal role in controlling the degree of the adsorption time effect.

Conclusions

In summary, we have designed and synthesized a new series of arylamine organic dyes bearing an N-heterocycle-substituted DTP spacer for iodine-free DSCs. The introduction of N-heterocycle-substituted DTP units for constructing organic dyes has dual functional effects, that is, tuning the charge-transfer excitation of the dyes and retarding the charge recombination in DSCs. In conjunction with the cobalt

Table 4 The relative CB positions, dye load amount and electron lifetime of the DSCs studied

Dye	ΔE_c[a]/mV	$\Gamma/10^{-7}$ mol cm^{-2}	Relative dye load amount[b]	Relative electron lifetime[c]
XS58/12 h	0	0.56	1	1
XS58/36 h	+12	0.64	1.14 fold	10 fold
XS59/12 h	0	0.63	1	1
XS59/36 h	+30	0.80	1.27 fold	8.7 fold
XS60/12 h	0	0.42	1	1
XS60/36 h	+6	0.45	1.07 fold	1.5 fold
XS61/12 h	0	0.64	1	1
XS61/36 h	+32	0.76	1.19 fold	2.0 fold

[a] The ΔE_c values were determined by the Q–V_{OC} plots. The CB positions of the DSCs for 12 hours of adsorption were set as zero. A positive value indicates a downwards CB shift. [b] The dye load amount of the DSCs for 12 hours adsorption was set as 1. [c] The electron lifetimes of the DSCs for 12 hours adsorption were set as 1. Relative electron lifetimes of DSCs for 36 hours adsorption relative to those of the 12 hours were calculated at a fixed charge density, namely 50 μC cm^{-2}.

electrolyte, XS58 and XS59 featuring dihexylaniline and hexylcarbazole substituted DTP spacers yielded PCEs of 8.14 and 8.20%, respectively, at the 100 mW cm^{-2}, simulated AM1.5 conditions. Moreover, the effect of the dye adsorption time on the performance of the iodine-free DSCs was investigated. The PCE values increased with increasing dye absorption time, the highest values being obtained with the films stained for 36 hours. Specifically, a significant effect of the dye adsorption time on the cells made with XS58 and XS59 was observed. At the same charge density, the electron lifetime of the 36 hour cells made with XS58 and XS59 was longer than that of the 12 hour cells by 10- and 8.7-fold, respectively. This indicates that the performance of XS58 and XS59 was strongly dependent upon the adsorption time. In contrast, the performance of XS60 and XS61 was found to be only weakly dependent upon the dye adsorption time. The joint IMVS and sensitized electrodes absorption experiments revealed that the structure of the DTP spacer is the key determinant of the degree of adsorption time effect. This finding provides important new insight into the effect of the dye structure on the photovoltaic performance of the iodine-free DSCs. From our findings, we propose that organic dyes with a strong ability for retarding charge recombination should be preferred in exploring this adsorption time effect for iodine-free DSCs.

Acknowledgements

We gratefully acknowledge the financial support from the National Natural Science Foundation of China (21003096, 21072152) and the Tianjin Natural Science Foundation (13JCZDJC32400).

Notes and references

1 B. O'Regan and M. Grätzel, *Nature*, 1991, **353**, 737–740.
2 A. Hagfeldt, G. Boschloo, L. Sun, L. Kloo and H. Pettersson, *Chem. Rev.*, 2010, **110**, 6595–6663.
3 Y.-S. Yen, H.-H. Chou, Y.-C. Chen, C.-Y. Hsu and J. T. Lin, *J. Mater. Chem.*, 2012, **22**, 8734–8747.
4 K.-L. Wu, W.-P. Ku, J. N. Clifford, E. Palomares, S.-T. Ho, Y. Chi, S.-H. Liu, P.-T. Chou, M. K. Nazeeruddin and M. Grätzele, *Energy Environ. Sci.*, 2013, **6**, 859–870.
5 Y. Shi, M. Liang, L. Wang, H. Han, L. You, Z. Sun and S. Xue, *ACS Appl. Mater. Interfaces*, 2013, **5**, 144–153.
6 L.-L. Li and E. W.-G. Diau, *Chem. Soc. Rev.*, 2013, **42**, 291–304.
7 (*a*) S. H. Kang, I. T. Choi, M. S. Kang, Y. K. Eom, M. J. Ju, J. Y. Hong, H. S. Kang and H. K. Kim, *J. Mater. Chem. A*, 2013, **1**, 3977–3982; (*b*) M. S. Kang, S. H. Kang, S. G. Kim, I. T. Choi, J. H. Ryu, M. J. Ju, D. Cho, J. Y. Lee and H. K. Kim, *Chem. Commun.*, 2012, **48**, 9349–9351.
8 (*a*) L. Favereau, J. Warnan, F. B. Anne, Y. Pellegrin, E. Blart, D. Jacquemin and F. Odobel, *J. Mater. Chem. A*, 2013, **1**, 7572–7575; (*b*) J. Warnan, Y. Pellegrin, E. Blart and F. Odobel, *Chem. Commun.*, 2012, **48**, 675–677.
9 M. Liang and J. Chen, *Chem. Soc. Rev.*, 2013, **42**, 3453–3488.
10 Y. Wu and W. Zhu, *Chem. Soc. Rev.*, 2013, **42**, 2039–2058.
11 H. Li, T. M. Koh, A. Hagfeldt, M. Grätzel, S. G. Mhaisalkar and A. C. Grimsdale, *Chem. Commun.*, 2013, **49**, 2409–2411.
12 F. Yang, M. Akhtaruzzaman, A. Islam, T. Jin, A. El-Shafei, C. Qin, L. Han, K. A. Alamry, S. A. Kosa, M. A. Hussein, A. M. Asirie and Y. Yamamotoae, *J. Mater. Chem.*, 2012, **22**, 22550–22557.
13 H. M. Song, K. D. Seo, M. S. Kang, I. T. Choi, S. K. Kim, Y. K. Eom, J. H. Ryu, M. J. Ju and H. K. Kim, *J. Mater. Chem.*, 2012, **22**, 3786–3794.
14 M. Lu, M. Liang, H. Han, Z. Sun and S. Xue, *J. Phys. Chem. C*, 2011, **115**, 274–281.
15 G. Li, M. Liang, H. Wang, Z. Sun, L. Wang, Z. H. Wang and S. Xue, *Chem. Mater.*, 2013, **25**, 1713–1722.
16 W. H. Zhu, Y. Wu, S. Wang, W. Li, X. Li, J. Chen, Z. S. Wang and H. Tian, *Adv. Funct. Mater.*, 2011, **21**, 756–763.
17 Z. S. Wang, N. Koumura, Y. Cui, M. Takahashi, H. Sekiguchi, A. Mori, T. Kubo, A. Furube and K. Hara, *Chem. Mater.*, 2008, **20**, 3993–4003.
18 R. Chen, X. Yang, H. Tian, X. Wang, A. Hagfeldt and L. Sun, *Chem. Mater.*, 2007, **19**, 4007–4015.
19 Y. Hong, J.-Y. Liao, D. Cao, X. Zang, D.-B. Kuang, L. Wang, H. Meier and C.-Y. Su, *J. Org. Chem.*, 2011, **76**, 8015–8021.
20 M. Velusamy, K. R. J. Thomas, J. T. Lin, Y.-C. Hsu and K.-C. Ho, *Org. Lett.*, 2005, **7**, 1899–1902.
21 H. J. Chen, H. Huang, X. W. Huang, J. N. Clifford, A. Forneli, E. Palomares, X. Y. Zheng, L. P. Zheng, X. Y. Wang, P. Shen, B. Zhao and S. T. Tan, *J. Phys. Chem. C*, 2010, **114**, 3280–3286.
22 Q. Q. Li, J. Shi, H. Y. Li, S. Li, C. Zhong, F. L. Guo, M. Peng, J. L. Hua, J. G. Qina and Z. Li, *J. Mater. Chem.*, 2012, **22**, 6689–6696.
23 Z. Yu, M. Gorlov, J. Nissfolk, G. Boschloo and L. Kloo, *J. Phys. Chem. C*, 2010, **114**, 10612–10620.
24 T. P. Chou, Q. Zhang, B. Russo, G. E. Fryxell and G. Cao, *J. Phys. Chem. C*, 2007, **111**, 6296–6302.
25 Z. Sun, R. Zhang, H. Xie, H. Wang, M. Liang and S. Xue, *J. Phys. Chem. C*, 2013, **117**, 4364–4373.
26 G. L. Zhang, Y. Bai, R. Z. Li, D. Shi, S. Wenger, S. M. Zakeeruddin, M. Grätzel and P. Wang, *Energy Environ. Sci.*, 2009, **2**, 92–95.
27 X. Hao, M. Liang, X. Cheng, X. Pian, Z. Sun and S. Xue, *Org. Lett.*, 2011, **13**, 5424–5427.
28 P. Gao, H. N. Tsao, M. Grätzel and M. K. Nazeeruddin, *Org. Lett.*, 2012, **14**, 4330–4333.
29 E. Longhi, A. Bossi, G. D. Carlo, S. Maiorana, F. D. Angelis, P. Salvatori, A. Petrozza, M. Binda, V. Roiati, P. R. Mussini, C. Baldoli and E. Licandro, *Eur. J. Org. Chem.*, 2013, **1**, 84–94.
30 H. Qin, S. Wenger, M. Xu, F. Gao, X. Jing, P. Wang, S. M. Zakeeruddin and M. Grätzel, *J. Am. Chem. Soc.*, 2008, **130**, 9202–9203.
31 W. Zeng, Y. Cao, Y. Bai, Y. Wang, Y. Shi, M. Zhang, F. Wang, C. Pan and P. Wang, *Chem. Mater.*, 2010, **22**, 1915–1925.
32 Y. M. Cao, N. Cai, Y. L. Wang, R. Z. Li, Y. Yuan and P. Wang, *Phys. Chem. Chem. Phys.*, 2012, **14**, 8282–8286.
33 A. Yella, R. Humphry-Baker, B. F. E. Curchod, N. A. Astani, J. Teuscher, L. E. Polander, S. Mathew, J.-E. Moser, I. Tavernelli, U. Rothlisberger, M. Grätzel, M. K. Nazeeruddin and J. Frey, *Chem. Mater.*, 2013, **25**, 2733–2739.

34 H. Zhou, L. Yang and W. You, *Macromolecules*, 2012, **45**, 607–932.
35 D. Sahu, H. Padhy, D. Patra, J.-F. Yin, Y.-C. Hsu, J.-T. Lin, K.-L. Lu, K.-H. Wei and H.-C. Lin, *Tetrahedron*, 2011, **67**, 303–311.
36 M. Xu, M. Zhang, M. Pastore, R. Li, F. De Angelis and P. Wang, *Chem. Sci.*, 2012, **3**, 976–983.
37 N. Cai, J. Zhang, M. Xu, M. Zhang and P. Wang, *Adv. Funct. Mater.*, 2013, **23**, 3539–3547.
38 J. Zhang, Z. Yao, Y. Cai, L. Yang, M. Xu, R. Li, M. Zhang, X. Dong and P. Wang, *Energy Environ. Sci.*, 2013, **6**, 1604–1614.
39 Z. H. Wang, M. Liang, L. Wang, Y. Hao, C. Wang, Z. Sun and S. Xue, *Chem. Commun.*, 2013, **49**, 5748–5750.
40 L. E. Polander, A. Yella, J. Teuscher, R. Humphry-Baker, B. F. E. Curchod, N. A. Astani, P. Gao, J.-E. Moser, I. Tavernelli, U. Rothlisberger, M. Grätzel, M. K. Nazeeruddin and J. Frey, *Chem. Mater.*, 2013, **25**, 2642–2648.
41 X. Cheng, M. Liang, S. Sun, Y. Shi, Z. Ma, Z. Sun and S. Xue, *Tetrahedron*, 2012, **68**, 5375–5385.
42 M. K. Kashif, J. C. Axelson, N. W. Duffy, C. M. Forsyth, C. J. Chang, J. R. Long, L. Spiccia and U. Bach, *J. Am. Chem. Soc.*, 2012, **134**, 16646–16653.
43 S. M. Feldt, E. A. Gibson, E. Gabrielsson, L. Sun, G. Boschloo and A. Hagfeldt, *J. Am. Chem. Soc.*, 2010, **132**, 16714–16724.
44 X. P. Zong, M. Liang, C. R. Fan, K. Tang, G. Li, Z. Sun and S. Xue, *J. Phys. Chem. C*, 2012, **116**, 11241–11250.
45 X. P. Zong, M. Liang, T. Chen, J. N. Jia, L. N. Wang, Z. Sun and S. Xue, *Chem. Commun.*, 2012, **48**, 6645–6647.
46 M. Wang, C. Grätzel, S. M. Zakeeruddin and M. Grätzel, *Energy Environ. Sci.*, 2012, **5**, 9394–9405.
47 J. Cong, X. Yang, L. Kloob and L. Sun, *Energy Environ. Sci.*, 2012, **5**, 9180–9194.
48 N. W. Duffy, L. M. Peter, R. M. G. Rajapakse and K. G. U. Wijayantha, *J. Phys. Chem. B*, 2000, **104**, 8916–8919.
49 G. Schlichthörl, S. Y. Huang, J. Sprague and A. J. Frank, *J. Phys. Chem. B*, 1997, **101**, 8141–8155.
50 G. Schlichthörl, N. G. Park and A. J. Frank, *J. Phys. Chem. B*, 1999, **103**, 782–791.
51 F. Sauvage, J.-D. Zhang, M. Zhang, S. M. Zakeeruddin, P. Comte, M. Nazeeruddin, P. Wang and M. Grätzel, *J. Am. Chem. Soc.*, 2011, **133**, 9304–9310.
52 N. Cai, R. Li, Y. Wang, M. Zhang and P. Wang, *Energy Environ. Sci.*, 2013, **6**, 139–147.
53 S. Rühle, M. Greenshtein, S. G. Chen, A. Merson, H. Pizem, C. S. Sukenik, D. Cahen and A. Zaban, *J. Phys. Chem. B*, 2005, **109**, 18907–18913.